

Dilution with Digital Microfluidic Biochips: How Unbalanced Splits Corrupt Target-Concentration

Sudip Poddar, Robert Wille, Hafizur Rahaman, and Bhargab B. Bhattacharya

Abstract—Sample preparation is an indispensable component of almost all biochemical protocols, and it involves, among others, making dilutions and mixtures of fluids in certain ratios. Recent microfluidic technologies offer suitable platforms for automating dilutions on-chip, and typically on a digital microfluidic biochip (DMFB), a sequence of (1 : 1) mix-split operations is performed on fluid droplets to achieve the target concentration factor (CF) of a sample. An (1 : 1) mixing model ideally comprises mixing of two unit-volume droplets followed by a (balanced) splitting into two unit-volume daughter-droplets. However, a major source of error in fluidic operations is due to unbalanced splitting, where two unequal-volume droplets are produced following a split. Such volumetric split-errors occurring in different mix-split steps of the reaction path often cause a significant drift in the target- CF of the sample, the precision of which cannot be compromised in life-critical assays. In order to circumvent this problem, several error-recovery or error-tolerant techniques have been proposed recently for DMFBs. Unfortunately, the impact of such fluidic errors on a target- CF and the dynamics of their behavior have not yet been rigorously analyzed. In this work, we investigate the effect of multiple volumetric split-errors on various target- CF s during sample preparation. We also perform a detailed analysis of the worst-case scenario, i.e., the condition when the error in a target- CF is maximized. This analysis may lead to the development of new techniques for error-tolerant sample preparation with DMFBs without using any sensing operation.

Keywords—Algorithmic microfluidics, embedded systems, fault-tolerance, healthcare devices, lab-on-chip.

I. INTRODUCTION

A digital microfluidic biochip (DMFB) is capable of executing multiple tasks of biochemical laboratory protocols in an efficient manner. DMFBs support droplet-based operations on a single chip with high sensitivity and reconfigurability. Discrete volume (nanoliter/picoliter) droplets are manipulated on DMFBs through electrical actuation on an electrode array [1]. Various fluid-handling operations such as dispensing, transport, mixing, split, dilution can be performed on these tiny chips with higher speed and reliability. Due to their versatile properties, these programmable chips are used in many

applications such as *in-vitro* diagnostics (point-of-care, self-testing), drug discovery (high-throughput screening), biotechnology (process monitoring, process development), ecology (agriculture, environment, homeland security), and sample preparation [2]–[6].

Sample preparation imparts significant impact on accuracy, assay-completion time and cost, and plays a pivotal role in biomedical engineering and life science [7]. It involves dilution or mixture preparation and comprises a sequence of mixing steps necessary to produce a mixture of input reagents having a desired ratio of the constituents. Note that sample collection, transportation, and preparation consume up to 90% cost and 95% of time [8]. In last few years, a large number of sample-preparation algorithms had been developed for reducing assay-completion time and cost [6], [9]–[15], based on the (1:1) mixing model and similar. In the conventional (1:1) mixing model, two unit-volume of droplets are mixed together and split into two equal-sized daughter droplets following the mixing operation. These algorithms output a particular sequence of mix-split operations (represented as a sequencing graph) in order to dilute the target-droplet to a desired target-concentration. For the convenience of dilution algorithms, a concentration factor (CF) is approximated with a binary fraction, which is reachable and satisfies a user-defined error-tolerance limit. The detailed description of sample preparation can be found elsewhere [16].

Although droplet-based microfluidic biochips enable the integration of fluid-handling operations and outcome sensing on a single biochip, errors are likely to occur during fluidic operations due to various permanent faults (e.g., dielectric breakdown or charge trapping), or transient faults (e.g., unbalanced split due to imperfect actuation). For example, two daughter-droplets may be of different volume after split-operation while executing mix-split steps on a DMFB platform. The unequal-volume droplets produced after an erroneous mix-split step, when used later will negatively impact the correctness of the desired target- CF . Therefore, unbalanced-split errors pose a significant threat to sample preparation. Hence, from the viewpoint of error-management, it is essential to introduce some error-management scheme to handle such faults during sample preparation.

In this paper, we focus especially on volumetric split-errors and investigate their effects on the target- CF during sample preparation. Split-errors may unexpectedly occur in any mix-split step of the mixing-path during sample preparation, thus affecting the concentration factor (CF) of the target-droplet [8]. Moreover, due to the unpredictable characteristics of fluidic-droplets, a daughter droplet of larger or smaller size may be

S. Poddar is with the Advanced Computing and Microelectronics Unit, Indian Statistical Institute, Kolkata, India 700108. Email: sudippoddar2006@gmail.com

Bhargab B. Bhattacharya is with the Department of Computer Science & Engineering, Indian Institute of Technology Kharagpur, India 721 302; this work was done while he had been with Indian Statistical Institute, Kolkata, India 700108. Email: bhargab.bhatta@gmail.com.

H. Rahaman is with the School of VLSI Technology, Indian Institute of Engineering Science and Technology, Shibpur, India 711103. E-mail: hafizur@vlsi.iiests.ac.in.

R. Wille is with the Institute for Integrated Circuits, Johannes Kepler University Linz, Austria. E-mail: robert.wille@jku.at.

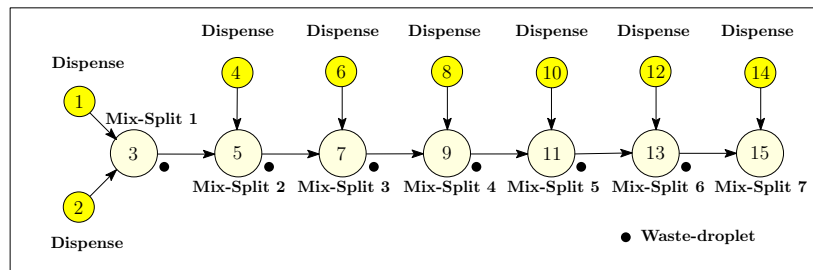


Fig. 1. Initial sequencing graph.

used in the mixing path following an erroneous split operation¹ on the mixing-path. Although a number of cyber-physical based approaches have been proposed for error-recovery [7], [17]–[20], they do not provide any guarantee on the number of rollback iterations that are needed to rectify the error. Thus, most of the prior approaches to error-recovery in biochips are non-deterministic in nature. On the other hand, the approach proposed in [8] performs error-correction in a deterministic sense; however, it assumes only the presence of single split-errors while classifying them as being *critical* or *non-critical*. A split-error occurring at a particular step is called *critical* (*non-critical*), if a single split-error when inserted at the corresponding step, causes the target-*CF* to exceed (bound within) the allowable error-tolerance range. This approach does not consider the possibility of multiple split-errors during classification. Furthermore, in a cyber-physical settings, it requires some additional time for sensing the occurrence of a *critical* error, if any, at every such step. Hence, when the number of critical errors becomes large, sensing time may outweigh the gain obtained in roll-forwarding assay-time, and as a result, we may need a longer overall execution time compared to that of the proposed method.

In this paper, we present a thorough analysis of the impact of multiple split-errors on a given target-*CF*. Based on these observations, methods for sample preparation that can deal with split errors even without any sensors and/or rollback can be derived. In fact, the findings discussed in this paper yield a method (described in [16]) that produces a target-*CF* within the allowable error-tolerance limit without using any sensor.

The remainder of the paper is organized as follows. Section II introduces the basic principle of earlier error-recovery approaches. We describe the effect of one or more volumetric split-errors on the target-*CF*, in Section III. Section IV presents the worst-case scenario, i.e., when *CF*-error in the target-droplet becomes maximum. A justification behind the maximum *CF*-error is then reported in Section V. Finally, we draw our conclusions in Section VI.

II. ERROR-RECOVERY APPROACHES: PRIOR ART

Earlier approaches perform error-recovery operations by repeating the concerned operations of the bioassay [21] for producing the target concentration factor within the allowable error-range. For example, all mix-split operations and dispensing operations of the initial sequencing graph (shown in Fig. 1)

¹depending on the selection of the erroneous droplet (larger or smaller volume) to be used in a subsequent step.

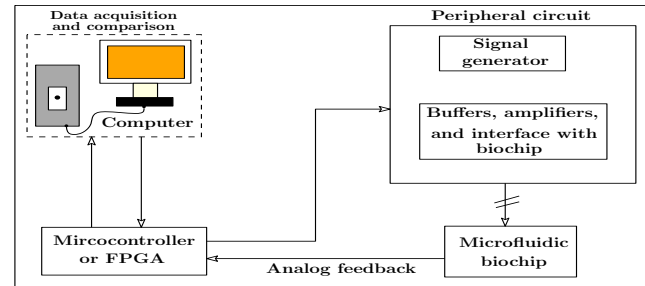


Fig. 2. Schematic of a cyberphysical error-recovery system.

were re-executed when an error is detected at the end (after execution of the bio-assay). However, the repetition of such experiments leads to wastage of precious reagents and hard-to-obtain samples, and results in longer assay completion-time.

A. Cyber-physical technique for error-recovery

In order to avoid such repetitive execution of on-chip biochemical experiments, recently, cyber-physical DMFBs were proposed for obtaining the desired outcome [18]. A diagram of a cyber-physical biochip is shown in Fig. 2 for demonstration purpose. It consists of the following components: a computer, a single-board microcontroller or an FPGA, a peripheral circuit, and the concerned biochip. Two interfaces are required for establishing the connection between control software and hardware of the microfluidic system. The first interface is required for converting the output signal of the sensor to an input signal that feeds the control software installed on the computer. The second interface transforms the output of the control software into a sequence of voltage-actuation maps that activate the electrodes of the biochip. The error-recovery operation is executed by the control software running in the back-end.

B. Compilation for error-recovery

Note that cyber-physical based DMFBs need to constantly monitor the output of the intermediate mix-split operations at designated checkpoints using on-chip sensors (integrated with the biochip). The original actuation sequences are interrupted when an error is detected during the execution of a bioassay. At the same time, the recovery actions, e.g., the re-execution of corresponding dispensing and mixing operations is initiated to remedy the error. However, the error-recovery operations

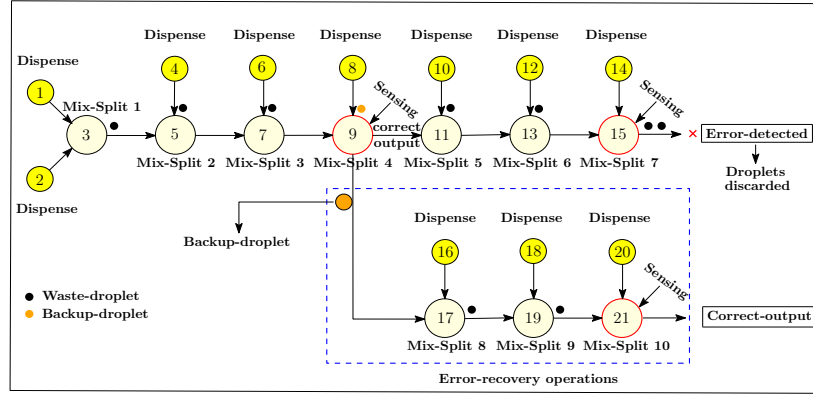


Fig. 3. Generation of a target-droplet by cyber-physical error-recovery approaches.

will have to be translated into electrode-actuation sequences in real-time.

The compilation of error-recovery actions can either be performed before actual execution of the bio-assay or during the execution of the bio-assay. So, depending on the compilation-time of operations, error-recovery approaches can be divided into two categories: i) offline (at design time), and ii) online (at run time).

In the offline approach, all possible errors of interest that might occur (under the assumed model) during the execution of a bio-assay are identified, and compilation is performed to pre-compute and store the corresponding error-recovery actuation sequences. They will provide an alternative schedule, which is stored in the memory. When an error is detected during actual execution of the bio-assay, the cyber-physical biochip executes the error-recovery actions by loading the corresponding schedules from the memory. However, this approach can be used to rectify only a limited number of errors (≤ 2) since a very large-size controller memory will be required to store the recovery sequences for all possible consequences of errors [19].

On the other hand, in the online approach, appropriate actions are carried out depending on the feedback given by the sensor. Compilation of error-recovery actions into electrode-actuation sequences is performed only at run-time.

C. Working principle of cyber-physical based DMFBs

In spite of the above difference, cyber-physical DMFBs perform error-recovery operations as follows. During actual execution of the bio-assay, a biochip receives control signals from the software running on the computer system. At the same time, the sensing system of the biochip sends a feedback signal to the software by processing it using field-programmable gate array (FPGA), or ASIC chips. If an error is detected by a sensor, the control software immediately discards the erroneous-droplet for preventing error-propagation, and performs the necessary error-recovery operations (i.e., corresponding actuation sequences are determined online/offline) for generating the correct output.

In order to produce the correct output, the outcome of the intermediate mix-split operations are verified using on-chip sensors suitably placed at designated checkpoints. For

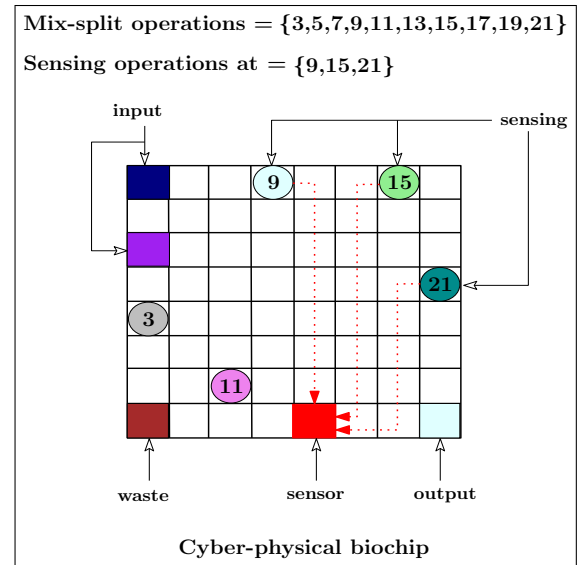


Fig. 4. Routing of droplets for sensing operation in a cyber-physical biochip.

example, in Fig. 3, the outcomes of *Mix-split 4* and *Mix-split 7* are checked by the sensor. When an error is detected, a portion of the bio-assay is re-executed. For instance, the operations shown within the blue box in Fig. 3 are re-executed when an error is detected at the last checkpoint. Note that the accuracy of a cyberphysical system also depends on the sensitivity of sensors. Unfortunately, due to cost constraints, only a limited number of sensors can be integrated into a DMFB [18]. Additionally, in order to check the status of intermediate droplets, they need to be routed to a designated sensor location on the chip. This may introduce a significant latency to the overall assay-completion time (Fig. 4). As a result, prior cyber-physical based error-recovery methods for sample preparation become expensive in terms of assay-completion time and reagent cost.

To summarize, cyber-physical error-recovery methods suffer from the following shortcomings:

- They are expensive in terms of assay-completion time and reagent-cost. Hence, they are unsuitable for field deployment and point-of-care testing in resource-constrained areas.

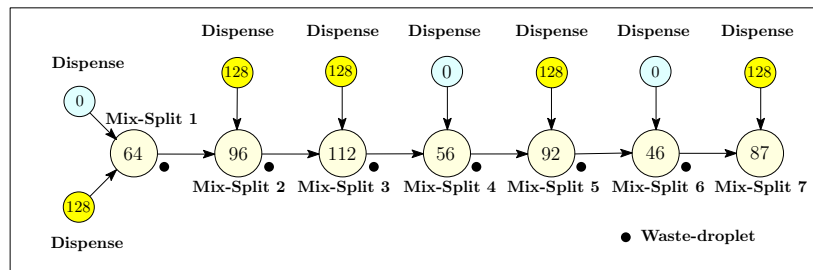


Fig. 5. Sequence of mix-split operations for the target- $CF = \frac{87}{128}$.

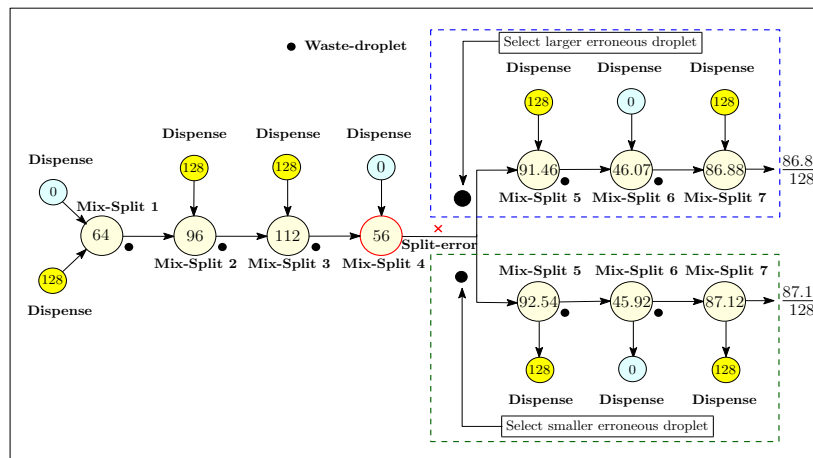


Fig. 6. Effect of choosing larger-/smaller-volume erroneous droplet on the target- $CF = \frac{87}{128}$.

- Prior cyberphysical solutions fail to provide any guarantee on the number of rollback attempts, i.e., how many iterations will be required to correct the error. Hence, error-recovery becomes non-deterministic.
- Each component used in the design of cyberphysical coupling may become a possible source of failure, which ultimately reduces the reliability of the biochip.

Now, we present below a detailed analysis of multiple volumetric split-errors and their effects on a target- CF .

III. EFFECT OF SPLIT-ERRORS ON THE TARGET CONCENTRATION

Generally, in the (1:1) mixing model (where two 1X-volume droplets are used for mixing operation), two 1X-volume daughter-droplets are produced after each mix-split operation. One of them is used in the subsequent mix-split operation and another one is discarded as waste droplet or stored for later use [6] (see Fig. 1). An erroneous mix-split operation may produce two unequal-volume droplets. Unless an elaborate sensing mechanism is used, it is not possible to predict which one of the resulting droplets (smaller/larger) is going to be used in the subsequent mix-split operation. Moreover, their effect on the target- CF becomes more complex when multiple volumetric split-errors occur in the mix-split path.

A. Single volumetric split-error

In order to analyze the effect of single volumetric split-error on the target- CF , we perform experiments with different

erroneous droplets and present the results in this section. We assume an example target- $CF = \frac{87}{128}$ of accuracy level = 7. The mix-split sequence that needs to be performed using *twoWayMix* algorithm [6] for generating the target- CF is shown in Fig. 5.

Let us consider the scenario of injecting 7% volumetric split-error at Mix-Split Step 4. Two unequal-volume daughter droplets are produced after this step when a split-error occurs. As stated earlier, it may not be possible to predict which droplet (smaller/larger) will be used for the mixing operation in the next step. The effect of the erroneous daughter droplet on the target- CF depends on the choice of the daughter-droplet to be used next. For example, the effect of 3% volumetric split-error (at Step 4) on the target- $CF = \frac{87}{128}$ is shown in Fig. 6. The effect of two errors on the target- CF (when the larger or smaller volume droplet is used at Mix-Split Step 4) is also shown in Fig. 6. The blue (green) box represents the scenario when the next operation is executed with the larger (smaller) erroneous droplet. It has been seen from Fig. 6 that the CF -error in the target increases when the smaller erroneous droplet is used in the mixing path compared to the use of the larger one.

Similarly, we perform further experiments for finding the effect of erroneous droplets on the target- CF . We report the results for volumetric split-error 3%, 5% and 7% occurring on the mixing path, in Table I. We observe that the CF -error in the target-droplet exceeds the error-tolerance limit in all cases when a volumetric split-error occurs in the last but one step. Moreover, the CF -error in the target- CF increases when the

TABLE I
IMPACT ON TARGET- $CF = \frac{87}{128}$ FOR DIFFERENT VOLUMETRIC SPLIT-ERRORS.

Volumetric split-error = 3%.				
Erroneous mix-split step	Selected-droplet		Target- $CF \times 128^*$	Within error-tolerance limit? ($CF\text{-error} \times 128 < 0.5?$)
	Larger	Smaller		
1	✓	×	86.98	Yes
1	×	✓	87.01	Yes
2	✓	×	87.01	Yes
2	×	✓	86.99	Yes
3	✓	×	87.04	Yes
3	×	✓	86.95	Yes
4	✓	×	86.88	Yes
4	×	✓	87.12	Yes
5	✓	×	87.04	Yes
5	×	✓	86.96	Yes
6	✓	×	86.39	No
6	×	✓	87.62	No
Volumetric split-error = 5%.				
Erroneous mix-split step	Selected-droplet		Target- $CF \times 128$	Within error-tolerance limit? ($CF\text{-error} \times 128 < 0.5?$)
	Larger	Smaller		
1	✓	×	86.98	Yes
1	×	✓	87.02	Yes
2	✓	×	87.01	Yes
2	×	✓	86.98	Yes
3	✓	×	87.08	Yes
3	×	✓	86.92	Yes
4	✓	×	86.81	Yes
4	×	✓	87.19	Yes
5	✓	×	87.06	Yes
5	×	✓	86.94	Yes
6	✓	×	86.00	No
6	×	✓	88.05	No
Volumetric split-error = 7%.				
Erroneous mix-split step	Selected-droplet		Target- $CF \times 128$	Within error-tolerance limit? ($CF\text{-error} \times 128 < 0.5?$)
	Larger	Smaller		
1	✓	×	86.97	Yes
1	×	✓	87.03	Yes
2	✓	×	87.02	Yes
2	×	✓	86.98	Yes
3	✓	×	87.11	Yes
3	×	✓	86.89	Yes
4	✓	×	86.73	Yes
4	×	✓	87.27	Yes
5	✓	×	87.09	Yes
5	×	✓	86.91	Yes
6	✓	×	85.61	No
6	×	✓	88.49	No

*: Results are shown up to two decimal places.

magnitude of volumetric split-error increases.

B. Multiple volumetric split-errors

To this end, we have analyzed the effect of single volumetric split-error on the target- CF (with different erroneous-volume

droplets) and observed that the CF -error in the target-droplet increases when the magnitude of split-error increases. However, due to unpredictable characteristics of fluid droplets, such split-errors may occur in multiple mix-split steps of the mixing path; they may change the CF of the desired target-droplet significantly. Moreover, volumetric split-errors may occur in any combination of signs (use of larger or smaller droplet following a split step) on the mixing path during sample preparation. We derive expressions that capture the overall effect of such errors on the target- CF .

Let ϵ_i indicate the percentage of the volumetric split-error occurring at the i^{th} mix-split step. A fundamental question in this context is the following: “How is the CF of a target-droplet affected by multiple volumetric split-errors $\{\epsilon_1, \epsilon_2, \dots, \epsilon_{i-1}\}$ occurring at different mix-split steps in the mixing path during sample preparation?”

In order to find a reasonable answer to the above question, let us consider the dilution problem for generating a target- $CF = C_t$ using *twoWayMix* [6] as shown in Fig. 7. Here, O_i represents the i^{th} (1:1) mix-split step, C_i is the resulting CF after the i^{th} mix-split step, and r_i is the CF of the source (100% for sample, 0% for buffer) used in i^{th} mix-split operation. Without loss of generality, let us assume that a volumetric split-error ϵ_i occurs after the i^{th} mix-split step of the mixing path, i.e., a two-unit volume droplet produces, after splitting, two daughter-droplets of volume $1+\epsilon$ and $1-\epsilon$, $\epsilon > 0$. Initially, sample and buffer are mixed at the first mix-split step (O_1). After this mixing operation, the CF and volume of the resulting droplet become $C_1 = \frac{P_0 \times (1 \pm \epsilon_0) + 2^{-1} \times r_0}{Q_0 \times (1 \pm \epsilon_0) + 2^{-1}}$ and $V_1 = \frac{Q_0 \times (1 \pm \epsilon_0) + 2^{-1}}{2^0}$, respectively, where $P_0 = Q_0 = \frac{1}{2}$, $\epsilon_0 = r_0 = 0$. Note that $r_i = 1$ (0) indicates whether a sample (buffer) is used in the i^{th} mix-split step of the mixing path. Furthermore, the sign $+$ ($-$) in the expression indicates whether a larger (smaller) droplet is used in the next mix-split step followed by a split operation.

A volumetric split-error may occur in one or more mix-split operations of the mixing path while preparing a target- CF . For example, volumetric split-errors $\{\epsilon_1, \epsilon_2, \dots, \epsilon_6\}$ may occur, one after another, in the mix-split operations $\{O_1, O_2, \dots, O_6\}$ as shown in Fig. 7. In Table II, we report the volume and concentration of the resulting daughter-droplets after each mix-split operation when all of the preceding steps suffer from split-errors.

Hence, for the occurrence of multiple volumetric split-errors, say $\{\epsilon_1, \epsilon_2, \epsilon_3, \dots, \epsilon_{i-2}, \epsilon_{i-1}\}$ at mix-split steps $\{O_1,$

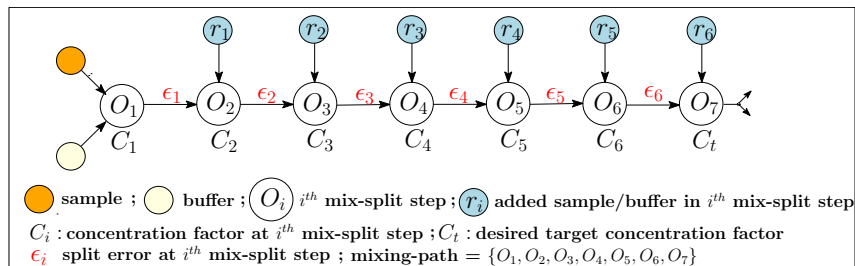


Fig. 7. Mix-split operations for generating target- $CF = C_t$ with accuracy level $n = 7$.

TABLE II
IMPACT OF SPLIT-ERRORS ON THE RESULTING DAUGHTER-DROPLETS.

Erroneous mix-split (O_i)	step	Split-error	\overline{CF}	\overline{V}	Parameter values
$\{O_1\}$		$\{\epsilon_1\}$	$C_2 = \frac{P_1 \times (1 \pm \epsilon_1) + r_1}{Q_1 \times (1 \pm \epsilon_1) + 2^0}$	$V_2 = \frac{Q_1 \times (1 \pm \epsilon_1) + 2^0}{2}$	$P_1 = P_0 \times (1 \pm \epsilon_0) + 2^{-1} \times r_0,$ $Q_1 = Q_0 \times (1 \pm \epsilon_0) + 2^{-1}$
$\{O_1, O_2\}$		$\{\epsilon_1, \epsilon_2\}$	$C_3 = \frac{P_2 \times (1 \pm \epsilon_2) + 2 \times r_2}{Q_2 \times (1 \pm \epsilon_2) + 2}$	$V_3 = \frac{Q_2 \times (1 \pm \epsilon_2) + 2}{2^2}$	$P_2 = P_1 \times (1 \pm \epsilon_1) + r_1,$ $Q_2 = Q_1 \times (1 \pm \epsilon_1) + 2^0$
$\{O_1, O_2, O_3\}$		$\{\epsilon_1, \epsilon_2, \epsilon_3\}$	$C_4 = \frac{P_3 \times (1 \pm \epsilon_3) + 2^2 \times r_3}{Q_3 \times (1 \pm \epsilon_3) + 2^2}$	$V_4 = \frac{Q_3 \times (1 \pm \epsilon_3) + 2^2}{2^3}$	$P_3 = P_2 \times (1 \pm \epsilon_2) + 2 \times r_2,$ $Q_3 = Q_2 \times (1 \pm \epsilon_2) + 2$
...
$\{O_1, O_2, O_3, O_4, O_5, O_6\}$		$\{\epsilon_1, \epsilon_2, \epsilon_3, \epsilon_4, \epsilon_5, \epsilon_6\}$	$C_7 = \frac{P_6 \times (1 \pm \epsilon_6) + 2^5 \times r_6}{Q_6 \times (1 \pm \epsilon_6) + 2^5}$	$V_7 = \frac{Q_6 \times (1 \pm \epsilon_6) + 2^5}{2^6}$	$P_6 = P_5 \times (1 \pm \epsilon_5) + 2^4 \times r_5,$ $Q_6 = Q_5 \times (1 \pm \epsilon_5) + 2^4$

\overline{CF} : Concentration of the resulting daughter-droplets after next mix-split step; \overline{V} : Volume of the resulting daughter-droplets after next mix-split step.

$O_2, O_3, \dots, O_{i-2}, O_{i-1}$, the CF and volume of the generated target-droplet after the final mix-split operation can be computed using the following expressions:

$$C_i = \frac{P_{i-1} \times (1 \pm \epsilon_{i-1}) + 2^{i-2} \times r_{i-1}}{Q_{i-1} \times (1 \pm \epsilon_{i-1}) + 2^{i-2}} \quad (1)$$

$$V_i = \frac{Q_{i-1} \times (1 \pm \epsilon_{i-1}) + 2^{i-2}}{2^{i-1}} \quad (2)$$

where $P_i = P_{i-1} \times (1 \pm \epsilon_{i-1}) + 2^{i-2} \times r_{i-1}$ and $Q_i = Q_{i-1} \times (1 \pm \epsilon_{i-1}) + 2^{i-2}$. In this way, the impact of multiple volumetric split-errors occurring on different mix-split steps of the mixing path on the target- CF can be precomputed.

In order to find the effect of multiple volumetric split-errors on the target- CF , we perform several experiments. We continue with the example target- $CF = \frac{87}{128}$ of accuracy level = 7, and inject 7% volumetric split-error simultaneously at different mix-split steps of the mixing path. The effects of such

split-errors are shown in Fig. 8. During simulation, we assume that the larger erroneous droplet is always used later when a split-error occurs in the mix-split path (i.e., ϵ is positive). For example, the effect of multiple 7% volumetric split-errors in Mix-Split Step 1 and Step 3 is shown in Fig. 8(b). Only the effect of three concurrent volumetric split-errors is also shown in Fig. 8 (c). It has been observed that CF -error in the target-droplet rapidly grows to $\frac{0.08}{128}$ and $\frac{0.17}{128}$ when two or three such split-errors are injected in the mix-split path.

IV. WORST-CASE ERROR IN THE TARGET- CF

So far we have analyzed the effect of multiple volumetric split-errors on a target- CF when a larger erroneous droplet is selected following each mix-split step. However, in a “sensor-free” environment, one cannot select the larger erroneous droplet at will for the subsequent operations. In reality, multiple volumetric split-errors may consist of an arbitrary

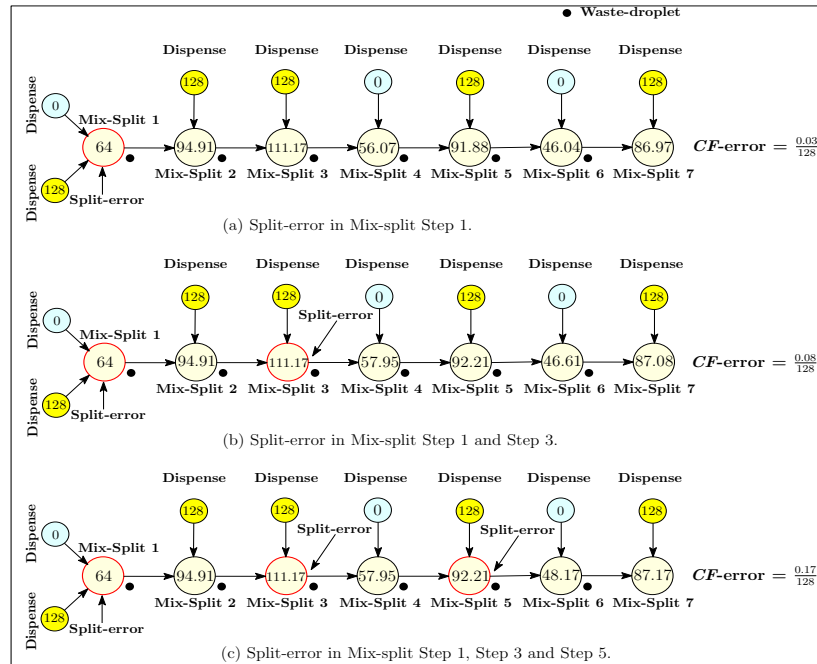


Fig. 8. Effect of multiple volumetric split-errors on the target- $CF = \frac{87}{128}$.

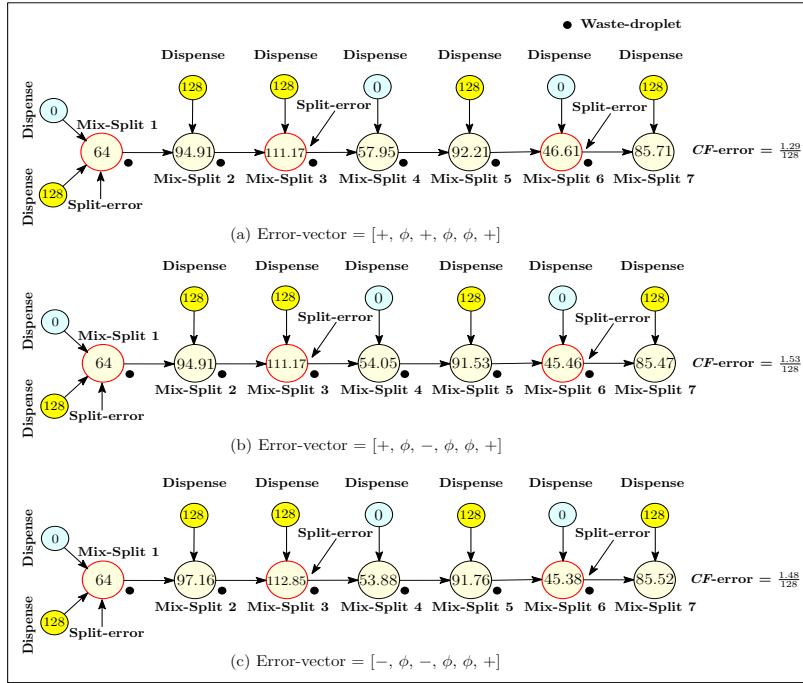


Fig. 9. Effect of multiple volumetric split-errors on the target- $CF = \frac{87}{128}$.

combination of large and small daughter-droplets. Hence, further analysis is required to reveal the role of such random occurrence of volumetric split-errors and their effects on the target- CF .

In order to facilitate the analysis, we define “error-vector” as follows: An error-vector of length k denotes the sequence of larger or smaller erroneous droplets, which are chosen corresponding to k mix-split errors in the mixing path. For example, an error-vector $[+, \phi, -, \phi, \phi, +]$ denotes volumetric split-error in Mix-Split Step 1, Step 3, and Step 6, where ϕ denotes no-error. In Step 1, the larger droplet is passed to the next step, whereas in Step 3, the smaller one is used in the next step, and so on. For k volumetric split-errors, 3^k error-vectors are possible. While executing actual mix-split operations, the target- CF can be affected by any one of them.

We perform simulated experiments for finding the effect of different error-vectors for the target- $CF = \frac{87}{128}$. Initially, we observe the effect of three errors corresponding to the mix-split operations {Mix-Split 1, Mix-Split 3, Mix-Split 6} to the target- CF (for 7% split-error). See Fig. 9 for an example.

We observe that CF -error in the target-droplet increases noticeably for the error-vectors $[+, \phi, +, \phi, \phi, +]$, $[+, \phi, -, \phi, \phi, +]$ and $[-, \phi, -, \phi, \phi, +]$ as depicted in the Fig. 9 (a)-(c). It has been seen from the Fig. 9 that CF -error exceeds the error-tolerance limit ($\frac{0.5}{128}$) in each cases. Thus target- CF is affected badly for these error-vectors. We also perform similar experiments with volumetric split-error 3% and found that CF -error decreases for all cases.

Moreover, we perform simulation for revealing the effect of remaining error-vectors on the target- CF and report the generated CF s by all possible error-vectors (# error-vectors = 8) in Table. III. It has been observed that the CF -error exceeds allowable error-tolerance limit in all such cases. On the other

TABLE III
EFFECT OF DIFFERENT ERROR-VECTORS ON THE TARGET- $CF = \frac{87}{128}$ FOR SPLIT-ERROR = 7%.

Error-vector	Produced $CF \times 128^*$	Produced $CF\text{-error} \times 128$	$CF\text{-error} \times 128 < 0.5?$
$[+, \phi, +, \phi, \phi, +]$	85.71	1.29	No
$[+, \phi, +, \phi, \phi, -]$	88.56	1.56	No
$[+, \phi, -, \phi, \phi, +]$	85.47	1.53	No
$[+, \phi, -, \phi, \phi, -]$	88.36	1.36	No
$[-, \phi, +, \phi, \phi, +]$	85.76	1.24	No
$[-, \phi, +, \phi, \phi, -]$	88.61	1.61	No
$[-, \phi, -, \phi, \phi, +]$	85.52	1.48	No
$[-, \phi, -, \phi, \phi, -]$	88.41	1.41	No

*: Results are shown up to two decimal places.

hand, the maximum CF -error in the target- CF occurs for the error-vector $[-, \phi, +, \phi, \phi, -]$ which is $\frac{1.61}{128}$ ($>$ error-tolerance limit).

Note that volumetric split-error may also occur in the remaining mix-split steps, i.e., each mix-split step of the mixing path may suffer from volumetric split-errors. Therefore, it is also essential to reveal the effect of multiple volumetric split-errors on the target- CF when an error occurs in each mix-split operation.

We further perform experiments to find the effect of such volumetric split-errors on the target- $CF = \frac{87}{128}$. The mix-split graph of the target- $CF = \frac{87}{128}$ consist of 7 mix-split operations (see Fig. 5). During simulation, we inject split-error in each mix-split step of the mixing path except the final mix-split operation (Mix-Split Step 7) since any volumetric split-error in the final mix-split operation will not alter the target- CF anymore (only the volumes of two resulting target-droplets may change). So there will be six potential mix-split steps (except the final one) where split-error can occur.

TABLE IV
EFFECT OF SOME ERROR-VECTORS OF LENGTH 6 ON THE TARGET- $CF = \frac{87}{128}$ FOR SPLIT-ERROR = 7%.

Error-vector	Produced $CF \times 128^*$	Produced $CF\text{-error} \times 128$	$CF\text{-error} \times 128 < 0.5?$
[+,+,+,+,+,+]	85.58	1.42	No
[+,-,+,+,+,+]	85.53	1.47	No
[+,-,-,+,+,+]	85.26	1.74	No
[+,-,+,+,-,+]	85.08	1.92	No
[-,+,-,-,+,-]	88.78	1.78	No
[-,+,-,-,-,-]	88.82	1.82	No
[-,+,-,-,-,-]	88.64	1.64	No
[-,-,-,-,-,-]	88.61	1.61	No

*: Results are shown up to two decimal places.

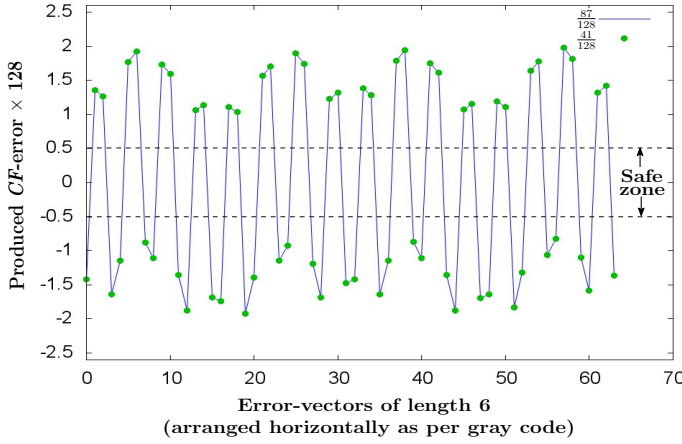


Fig. 10. Value of $(CF\text{-error} \times 128)$ for all possible error-vectors with 7% split-error for the target- $CF = \frac{41}{128}$ and $\frac{87}{128}$.

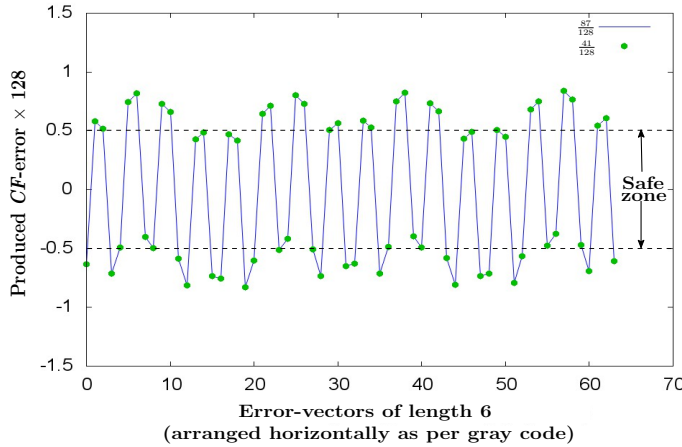


Fig. 11. Value of $(CF\text{-error} \times 128)$ for all possible error-vectors with 3% split-error for the target- $CF = \frac{41}{128}$ and $\frac{87}{128}$.

Thus, there will be 64 possible error-vectors. We set split-error = +0.07 or -0.07, in each mix-split step, depending on the sign of the error in the corresponding position of vector. We perform experiments exhaustively and report the results for some representative error-vectors for the target- $CF = \frac{87}{128}$ in Table IV. We see that the CF -error exceeds the allowable error-range in every case.

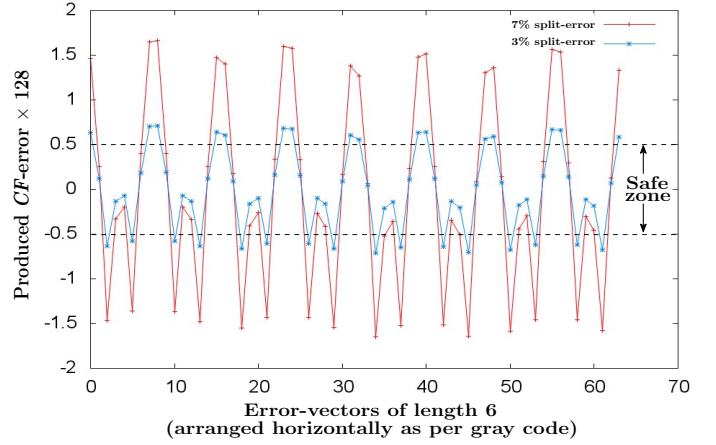


Fig. 12. Value of $(CF\text{-error} \times 128)$ for all possible error-vectors for 7% and 3% split-error for the target- $CF = \frac{17}{128}$.

We also show the CF -error by all possible error-vectors in Fig. 10 for the target- $CF = \frac{41}{128}$ and $\frac{87}{128}$ (complement of $\frac{41}{128}$) for demonstration purpose. We plot error-vectors (setting + \rightarrow 0, - \rightarrow 1) along the X-axis, and arrange them from left-to-right following a gray-code, so that any two adjacent vectors are only unit Hamming distance apart. The Y-axis shows the corresponding values of $CF\text{-error} \times 128$. Based on exhaustive simulation, we observe that the CF -error in both target- CF s becomes maximum (1.977) for the error-vector $[-,+,-,+,-,+,-]$ (at the 57th position on the X-axis). Note that for the target- $CF = \frac{41}{128}$, CF -errors are multiplied with -1 for the ease of analysis. We notice that none of these outcomes lies within the safe-zone (within error-tolerance limit). We also perform similar experiment for both the target- CF s when split-error becomes 3% and observe that for 12 cases, the errors lies within the tolerance zone, and the maximum CF -error reduces to $\frac{0.84}{128}$ corresponding to the same error-vector $[-,+,-,+,-,+,-]$ (Fig. 11) for both CF s. However, for the target- $CF = \frac{17}{128}$, a large number of CF -errors = 29 (32) generated by all possible error-vectors of length 6 lie within the error-tolerance zone for 7% (3%) split-errors (see Fig. 12). Note that the magnitude of CF -errors decreases in each case when split-error reduces to 3%.

We further perform simulation for measuring maximum CF -error generated for all target- CF s of accuracy level 7 (with 7% split-error). We plot the results in Fig. 13. We observe that the CF -error for the target- $CF = \frac{63}{128}$ and $\frac{65}{128}$ becomes maximum ($\frac{4.12}{128}$) compared to those produced by other error-vectors. The error-vector $[-,-,-,-,-,-,-]$ generates the maximum CF -error for both these target- CF s.

V. MAXIMUM CF -ERROR: A JUSTIFICATION

Motivated by the need for a formal proof for generating maximum CF -error in the target- CF , we have performed a rigorous theoretical analysis and further experiments to study the properties of CF -error in a target- CF . The following analysis, as shown below, reveals how the problem of error-tolerance can be handled in a more concrete fashion.

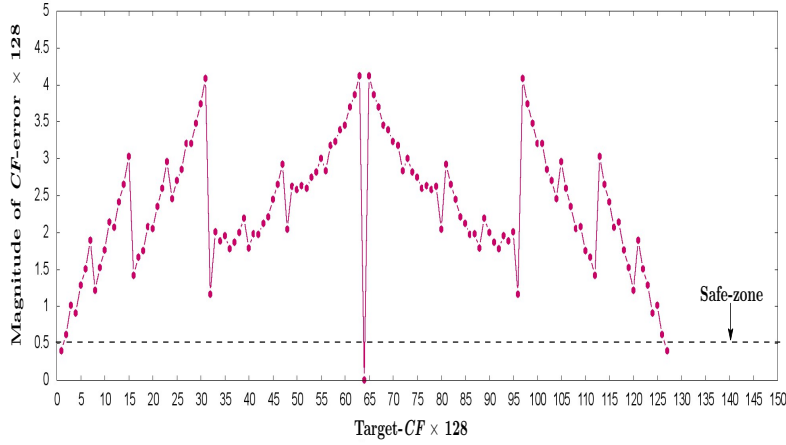


Fig. 13. Maximum value of $(CF\text{-error} \times 128)$ for all target- CF s with accuracy level = 7.

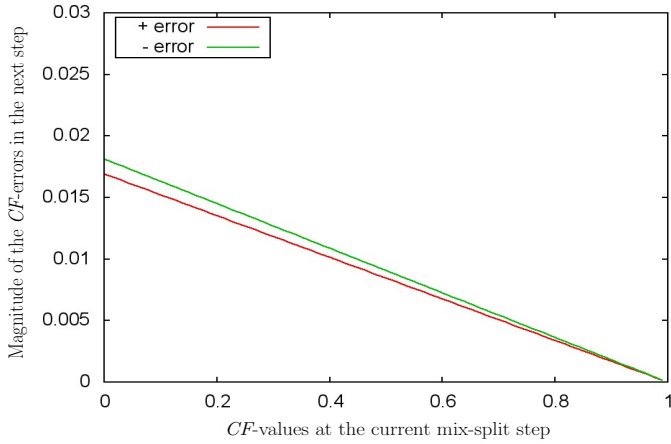


Fig. 14. CF -error at the next mix-split step (for positive and negative single split-error).

Consider a particular target- $CF = C_t$ and its dilution tree. Let the current mix-split step be i (other than the last step, where the occurrence of split-error does not matter), and the intermediate- CF arriving at i be C_i . If a 1X sample (buffer) droplet is added in this step, it produces $CF = \frac{C_i+1}{2}$ ($= \frac{C_i}{2}$), assuming that the volume of the droplet arriving at i is correct (1X).

Consider the first case, and assume that the droplet arriving at i suffers a volumetric split-error of magnitude ϵ at the previous step. Hence, after mixing with a sample droplet, the intermediate- CF will become: $\frac{C_i(1+\epsilon)+1}{2+\epsilon}$; the sign of ϵ is set to positive (negative) when the incoming intermediate-droplet is larger (smaller) than the ideal volume 1X. Thus, the error (E_r) in the intermediate- CF becomes:

$$E_r = \frac{C_i + 1}{2} - \frac{C_i(1 + \epsilon) + 1}{2 + \epsilon} = \frac{\epsilon(1 - C_i)}{4 + 2\epsilon} \quad (3)$$

From Equation 3, it can be observed that the magnitude of E_r becomes larger when ϵ is negative, because a negative error reduces the value of the denominator. In other words, the error in CF will be more if a droplet of smaller-volume arrives at Step i compared to the case when a larger-volume droplet

arrives at the mixer. In other words, the *effect of the error is not symmetrical*; however, since the volumes of the two daughters will be proportionately different as well, when they are mixed, the error is canceled. We perform an experiment assuming volumetric error (7%), i.e., by setting $\epsilon = +0.07$ or -0.07 in one mix-split step, for all values of intermediate- CF s. The corresponding results are shown in Fig. 14. It can be observed that a negative split-error always produces larger CF -error in the target- CF for a single split-error (error-vector of length 1). Similar effects will be observed when a buffer droplet is mixed at Step i .

We also perform simulation by varying C_i from 0 to 1, and ϵ from -0.07 to 0.07 in Equation 3 and calculate CF -errors. We report the results as 3-dimensional (3D) plots (with different views) in Fig. 15 and Fig. 16, respectively. We observe that simulation results favorably match with theoretical results (see Fig. 14), i.e., the negative split-error (single) always produces larger CF -error for a single split-error. However, the effect of error on a target- CF becomes much more complicated when multiple split-errors are considered.

In order to demonstrate the intricacies, we have performed a representative analysis considering three consecutive split-errors. For simplicity, let us assume that an error of magnitude ϵ is injected in each of these three mix-split steps. Generalizing Equation 3, we can show that the corresponding CF -error observed after three steps will be:

$$E_r = \frac{(((C_i(1 + \epsilon) + r_1)(1 + \epsilon) + r_2))(1 + \epsilon) + r_3}{(((2 + (2 + \epsilon)(1 + \epsilon)))(1 + \epsilon) + 4) \frac{(C_i + r_1 + r_2 + r_3)}{8}}$$

where $r_i = 1$ (for sample droplet)
 $= 0$ (for buffer droplet), for Step i , $i = 1, 2, 3$.

As before, we assume that $\epsilon = +0.07$ or -0.07 , and since we have three consecutive split steps, we can have eight possible combinations of such error vectors $[\phi^\alpha, -, -, -, \phi^\beta]$, $[\phi^\alpha, -, -, +, \phi^\beta]$, \dots , $[\phi^\alpha, +, +, +, \phi^\beta]$ for a given combination of r_1, r_2, r_3 , where $0 \leq \alpha \leq (n - 4)$, $0 \leq \beta \leq (n - 4)$ and $\alpha + \beta + 3 = n - 1$ (n is the accuracy level). Thus, altogether, there will be

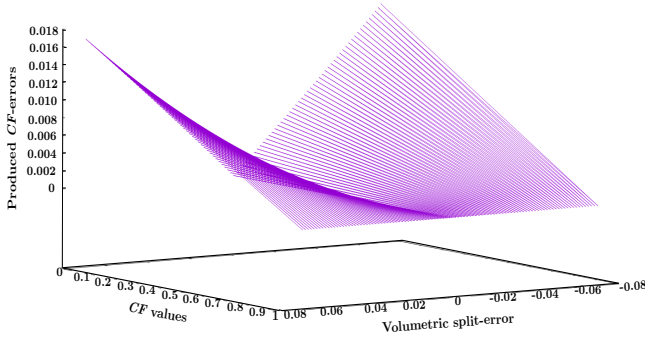


Fig. 15. CF -error at the next mix-split step (for positive and negative single split-error).

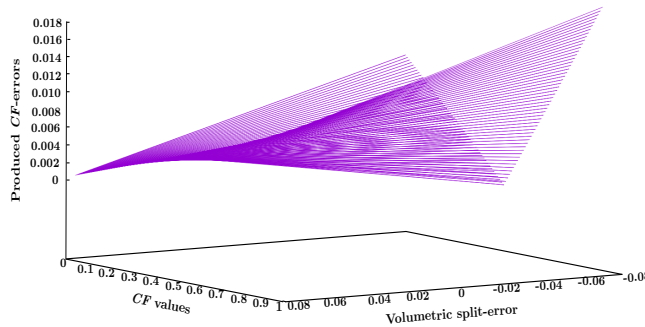


Fig. 16. CF -error at the next mix-split step (for positive and negative single split-error).

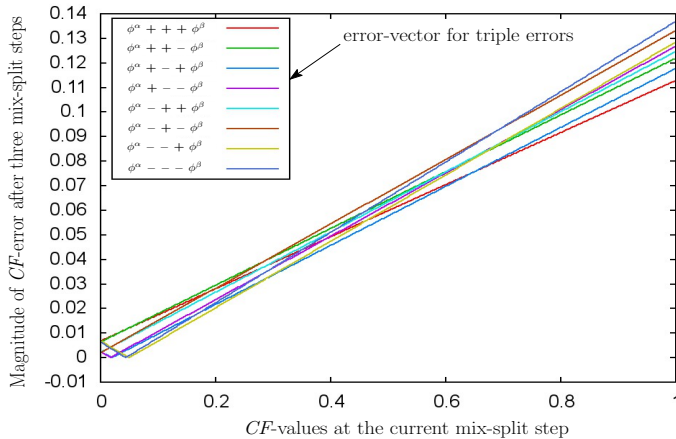


Fig. 17. CF -error for triple split-errors.

8 combinations. Fig. 17 shows the errors in CF observed after three consecutive split-errors by setting $r_1 = 0$, $r_2 = 1$, $r_3 = 1$, for all values of starting- CF , and for all eight combinations of error-vectors. From the nature of the plot, it is apparent that it is very hard to predict for which error-vector the maximum

CF -error will occur, even for a given combination of r -values. The maximum error depends on the CF -value from which the *critical*-split-section begins and also on the error-vector that is chosen (i.e., whether to proceed with the larger or the smaller daughter-droplet). Furthermore, the error-expression becomes increasingly complex when the number of split-errors becomes large.

As an example, we perform experiments to study the fluctuations of the error in a particular target- CF for all combinations of error-vectors and showed the plot in Fig. 10. Note that there are several peaks up and down in 10, and based on exhaustive simulation, the value of (maximum-error \times 128) is observed to be 1.977, which occurs for the error vector $[-, +, +, -, +, -]$ (at the 57th position on the X-axis in Fig. 10).

From the above analysis and experimental results, we conclude that it is hard to formulate a mechanism that will identify the exact “maximum-error-vector” without doing exhaustive simulation. In other words, it may not be possible to develop a procedure that will generate the maximum-error-vector without doing exhaustive analysis.

VI. CONCLUSION

In this paper, initially, we have analyzed the effect of single volumetric split-errors (using the larger- or smaller-volume erroneous daughter-droplet) and found both theoretically and experimentally that the CF -error in the target-droplet becomes larger when the smaller-volume daughter droplet is used in the assay, i.e., when ϵ becomes negative. We also observed that the CF -error in a target-droplet increases with increasing magnitude of the split-error. Next, we have performed various experiments to observe the effect of multiple CF -errors on the target- CF and noticed that it may be affected by any combination of erroneous droplets (smaller/larger) during the execution of mix-split operations. We also observed that the CF -error in a target-droplet increases when the target- CF is affected by a large number of split-errors. We performed rigorous analysis to identify the error vector that causes the maximum CF -error in the target-droplet. Unfortunately, it appears that it is very difficult to come up with an algorithmic solution for identifying an error vector that maximizes the CF -error in the target under multiple split-errors. But still, the observations and findings summarized in this paper will provide useful inputs to the development of methods for sample preparation that can deal with split errors even without any sensors and/or rollback (such as recently presented e.g. in [16], [22]).

REFERENCES

- [1] F. Mugele and J.-C. Baret, “Electrowetting: from basics to applications,” *Journal of Physics: Condensed Matter*, vol. 17, no. 28, pp. 705–774, 2005.
- [2] K. Chakrabarty and F. Su, *Digital Microfluidic Biochips - Synthesis, Testing, and Reconfiguration Techniques*. CRC Press, 2007.
- [3] V. Srinivasan, V. K. Pamula, and R. B. Fair, “An integrated digital microfluidic lab-on-a-chip for clinical diagnostics on human physiological fluids,” *Lab Chip*, vol. 4, pp. 310–315, 2004.
- [4] K. Chakrabarty, R. B. Fair, and J. Zeng, “Design tools for digital microfluidic biochips: Toward functional diversification and more than Moore,” *IEEE Trans. on CAD*, vol. 29, no. 7, pp. 1001–1017, 2010.
- [5] M. Alistar, P. Pop, and J. Madsen, “Redundancy Optimization for Error Recovery in Digital Microfluidic Biochips,” *Design Automation for Embedded Systems*, vol. 19, no. 1-2, pp. 129–159, 2015.

- [6] W. Thies, J. P. Urbanski, T. Thorsen, and S. P. Amarasinghe, "Abstraction layers for scalable microfluidic biocomputing," *Natural Computing*, vol. 7, no. 2, pp. 255–275, 2008.
- [7] Y.-L. Hsieh, T.-Y. Ho, and K. Chakrabarty, "Biochip Synthesis and Dynamic Error Recovery for Sample Preparation Using Digital Microfluidics," *IEEE Trans. on CAD*, vol. 33, no. 2, pp. 183–196, 2014.
- [8] S. Poddar, S. Ghoshal, K. Chakrabarty, and B. B. Bhattacharya, "Error-correcting sample preparation with cyberphysical digital microfluidic lab-on-chip," *ACM TODAES*, vol. 22, no. 1, pp. 2:1–2:29, 2016.
- [9] S. Roy, B. B. Bhattacharya, and K. Chakrabarty, "Optimization of dilution and mixing of biochemical samples using digital microfluidic biochips," *IEEE Trans. on CAD*, vol. 29, pp. 1696–1708, 2010.
- [10] J.-D. Huang, C.-H. Liu, and T.-W. Chiang, "Reactant minimization during sample preparation on digital microfluidic biochips using skewed mixing trees," in *Proc. of ICCAD*, 2012, pp. 377–384.
- [11] C.-H. Liu, T.-W. Chiang, and J.-D. Huang, "Reactant Minimization in Sample Preparation on Digital Microfluidic Biochips," *IEEE Trans. on CAD*, vol. 34, no. 9, pp. 1429–1440, 2015.
- [12] D. Mitra, S. Roy, S. Bhattacharjee, K. Chakrabarty, and B. B. Bhattacharya, "On-Chip Sample Preparation for Multiple Targets Using Digital Microfluidics," *IEEE Trans. on CAD*, vol. 33, no. 8, pp. 1131–1144, 2014.
- [13] S. Bhattacharjee, S. Poddar, S. Roy, J.-D. Huang, and B. B. Bhattacharya, "Dilution and mixing algorithms for flow-based microfluidic biochips," *IEEE Trans. on CAD*, vol. 36, no. 4, pp. 614–627, 2017.
- [14] Y.-L. Hsieh, T.-Y. Ho, and K. Chakrabarty, "A Reagent-Saving Mixing Algorithm for Preparing Multiple-Target Biochemical Samples Using Digital Microfluidics," *IEEE Trans. on CAD*, vol. 31, no. 11, pp. 1656–1669, 2012.
- [15] S. Bhattacharjee, R. Wille, J.-D. Huang, and B. Bhattacharya, "Storage-aware sample preparation using flow-based microfluidic lab-on-chip," in *Proc. of DATE*, 2018, pp. 1399–1404.
- [16] S. Poddar, R. Wille, H. Rahaman, and B. B. Bhattacharya, "Error-Oblivious Sample Preparation with Digital Microfluidic Lab-on-Chip," *IEEE Trans. on CAD*, 2018, doi: 10.1109/TCAD.2018.2864263.
- [17] Y. Zhao, T. Xu, and K. Chakrabarty, "Integrated control-path design and error recovery in the synthesis of digital microfluidic lab-on-chip," *ACM JETC*, vol. 6, no. 3, pp. 11:1–11:28, 2010.
- [18] Y. Luo, K. Chakrabarty, and T.-Y. Ho, "Error Recovery in Cyberphysical Digital Microfluidic Biochips," *IEEE Trans. on CAD*, vol. 32, no. 1, pp. 59–72, 2013.
- [19] —, "Real-time error recovery in cyberphysical digital-microfluidic biochips using a compact dictionary," *IEEE Trans. on CAD*, vol. 32, no. 12, pp. 1839–1852, 2013.
- [20] —, "Biochemistry Synthesis on a Cyberphysical Digital Microfluidics Platform Under Completion-Time Uncertainties in Fluidic Operations," *IEEE Trans. on CAD*, vol. 33, no. 6, pp. 903–916, 2014.
- [21] C. A. Mein, B. J. Barratt, M. G. Dunn, T. Siegmund, A. N. Smith, L. Esposito, S. Nutland, H. E. Stevens, A. J. Wilson, M. S. Phillips, N. Jarvis, S. Law, M. D. Arruda, and J. A. Todd, "Evaluation of single nucleotide polymorphism typing with invader on pcr amplicons and its automation," *Genome Research*, vol. 10, no. 3, pp. 330–343, 2000.
- [22] Z. Zhong, R. Wille, and K. Chakrabarty, "Robust sample preparation on low-cost digital microfluidic biochips," in *Proc. of ASP-DAC*, 2019.